Controlling local currents in molecular junctions

Hari Kumar Yadalam and Upendra Harbola
Department of Inorganic and Physical Chemistry, Indian Institute of Science, Bangalore 560012, India
(Received 14 June 2016; published 19 September 2016)

The effects of nonequilibrium constraints and dephasing on the circulating currents in molecular junctions are analyzed. Circulating currents are manifestations of quantum effects and can be induced either by externally applied bias or an external magnetic field through the molecular system. In a symmetric Aharonov-Bohm ring, bond currents have two contributions, bias driven and magnetic field driven. We analyze the competition between these two contributions and show that, as a consequence, current through one of the branches can be completely suppressed. We then study the effect of asymmetry (as a result of chemical substitution) on the current pathways inside the molecule and study asymmetry-induced circulating currents (without magnetic field) by tuning the coupling strength of the substituent (at finite bias).

DOI: 10.1103/PhysRevB.94.115424

I. INTRODUCTION

Persistent charge current is the current flowing in systems with ring geometries, due to the phase coherent motion of electrons [1]. It can be induced by the presence of vector potential due to magnetic fields threading the ring, first studied by Pauling in the context of aromatic molecules [2]. The effect of magnetic flux through superconducting disks was studied by Byers and Yang [3]. Buttiker *et al.* [4] showed that 1D metallic rings, where phase coherence of electrons is maintained, act like superconductors to produce a persistent current flowing in the ring. Further studies have explored the effects of various quantities such as disorder, temperature, and Coulomb interaction between electrons on the persistent current [1]. In this study we extend these works to the molecular regime in the molecular junction setup.

In recent years, the electron conduction through a single molecular junction has attracted a lot of research interest due to its fundamental interest in exploring quantum effects and its applications in miniaturization of electronic components (molecular electronics). The idea of molecular electronics is to control the electronic current by manipulating the physical and chemical properties of the molecule. Current flowing through molecules in a junction can take different pathways inside a molecule. These pathways have been studied recently [5].

The ability to control local currents can be useful from a technological perspective for developing new device functionalities. For example, we can have a quantum dot circuit which is capacitively coupled to one of the arms of a ring structure, current through which can be manipulated by changing magnetic flux threading the ring, thereby creating a magnetic switch. Further, it is useful to understand which pathways through the molecule are conducting the charge predominantly. It is interesting to note that it is possible to find the pathways which are actively conducting the charge through the molecule using inelastic electron tunneling spectroscopy [6]. This may allow us to engineer molecular circuits more efficiently. Here we analyze the local currents inside a molecular junction in the presence (in a symmetric junction) and absence (asymmetric junction) of the magnetic field.

Magnetic field threading the molecular ring induces different phases in the electron wave function as it transverses through different pathways inside the molecule. As we discuss below, this phase acquired by the electron affects both the local currents and the net current. Hence the dependence of current flow on magnetic flux allows us to control not only the net current through the junction but also the local bond currents inside the junction. Although much work has been done to study the effect of magnetic flux on current flowing between leads [5,7–9], little attention has been paid to the study of the effect of magnetic flux on the circulating currents inside the molecule in the presence of external bias, with the notable exceptions of Refs. [10–13]. Here we analyze the aspect of controlling the local currents by manipulating external magnetic field and chemical substitution. For a symmetric Aharonov-Bohm ring case, in the presence of the external bias, it is possible to fine-tune the magnetic flux to completely suppress current flow across different branches selectively. We show that the bond current has two contributions, which we identify as magnetic-field-driven and bias-driven contributions. These two contributions have different origins in the molecular eigenstate basis; the former contribution is due to the current carried by molecular eigenstates, while the latter is due to the coherences between eigenstates induced by the leads. These two contributions compete and may cancel each other along a branch, while adding up to enhance the current along the other branch. This is not possible if either the magnetic field or the bias is present alone. We further consider the case where an extra site is coupled to the ring system and demonstrate that a circulating current (in this work we adapt an intuitive definition of circulating current as "circulating current is present if the direction of current flowing through one of the branches is opposite to the direction of the net current, and its magnitude is given by the smallest of the currents flowing across the two branches") can also be induced by tuning the coupling strength of the substituent (at finite bias). This is due to the asymmetry induced between pathways by the extra coupling site. We derive analytic expressions for the bond currents and discuss them under different conditions. We find that the circulating currents can be induced not only by the magnetic field but also due to coupling with the leads (in the presence of asymmetry and finite bias). That is, the direction of the current flowing across a branch can be manipulated by tuning the coupling strength with the leads. We present a detailed analysis of bond currents based on analytical results.

The rest of the paper is organized as follows. In the next section (Sec. II) we consider a model with asymmetry in the presence of magnetic field and calculate the bond currents inside the molecule and the net current in the circuit. In Sec. III, we present a symmetric molecular ring system coupled to two metal leads in the presence of a magnetic flux. We discuss bond currents, net current, and the circulating current at equilibrium (when the two leads are at the same thermodynamic state) and nonequilibrium conditions. In Sec. IV we discuss circulating currents in an asymmetric molecular ring junction in the absence of the magnetic field. We conclude in Sec. V.

II. MODEL HAMILTONIAN AND CURRENT CALCULATIONS

A. Model Hamiltonian

To study the effect of asymmetry and magnetic fields on bond currents in ring molecular systems out of equilibrium (at steady state), we consider a simple model shown in Fig. 1. It consists of a ring molecular system with four identical localized sites (orbitals) coupled to nearest sites through hopping. Diagonally opposite sites are coupled to two metal leads, and one of the free sites is coupled to an extra site. Further, a magnetic flux is pierced through the molecular ring. All four sites forming the ring are taken to have the same energy (taken as zero by rescaling all other energies) and their coupling strengths to nearest neighbors are equal, taken as the energy unit. Specifically, sites 1 and 3 are coupled to the left and right metallic leads (modeled as free-electron reservoirs at thermal equilibrium), respectively. Site 2 is coupled to an extra site (site 5 with energy ϵ) with coupling strength t. The effect of the external magnetic field is included in the model Hamiltonian in the spirit of Peierls substitution [14]. In this work, we only consider noninteracting spinless electrons.

The Hamiltonian describing this model is given as

$$\hat{H} = \sum_{i,j=1}^{5} H_{0_{ij}} c_i^\dagger c_j + \sum_{\substack{k \\ \alpha=L,R}} \epsilon_{\alpha,k} d_{\alpha k}^\dagger d_{\alpha k} + \sum_k [g_L d_{Lk}^\dagger c_1 + g_R d_{Rk}^\dagger c_3 + \text{H.c.}], \tag{1}$$

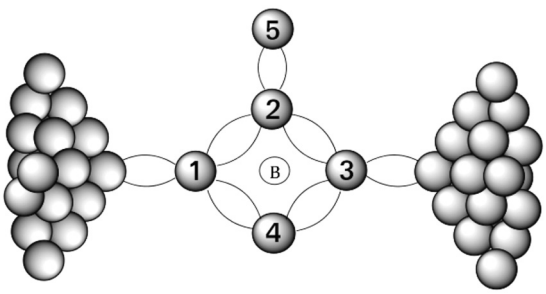

FIG. 1. Schematic of model system considered. It consists of four identical localized sites coupled to each other to form a ring geometry (with magnetic field piercing the ring); diagonally opposite sites are coupled to two metal leads and one of the sites not coupled to leads is coupled to an extra site.

where

$$H_0 = \begin{pmatrix} 0 & -e^{-i\frac{\phi}{4}} & 0 & -e^{i\frac{\phi}{4}} & 0 \\ -e^{i\frac{\phi}{4}} & 0 & -e^{-i\frac{\phi}{4}} & 0 & -t \\ 0 & -e^{i\frac{\phi}{4}} & 0 & -e^{-i\frac{\phi}{4}} & 0 \\ -e^{-i\frac{\phi}{4}} & 0 & -e^{i\frac{\phi}{4}} & 0 & 0 \\ 0 & -t & 0 & 0 & \epsilon \end{pmatrix} \tag{2}$$

is the single-particle Hamiltonian for the isolated molecule. ϕ is the dimensionless magnetic flux given by $(B \times A)/(\frac{\hbar c}{e})$, where B is the strength of applied magnetic field, A is the area of the molecular ring, and $\hbar$, c, e represent the reduced Planck's constant, speed of light, and (absolute) charge of an electron, respectively. Here c_i ($c_i^\dagger$) are the fermion annihilation (creation) operators for destroying (creating) an electron at site i and similarly $d_{\alpha k}$ ($d_{\alpha k}^\dagger$) are operators for destroying (creating) an electron in state k in the α lead ($\alpha = L/R$). The first two terms in the Hamiltonian represent free-system and free-lead Hamiltonians, and the third term represents hybridization between system and lead sites. We also assumed the wideband approximation (i.e., system lead hybridization is independent of k).

B. Bond currents

Expressions for bond current operators between localized sites can be obtained from the continuity equation for the charge density operator at any localized site. For example rate of change of charge at site 1, i.e.,

$$\frac{d}{dt}(-ec_1^\dagger c_1) = \frac{ie}{\hbar}[c_1^\dagger c_1, H], \tag{3}$$

gives three terms on the right-hand side, and each of these three terms can be identified as the operator for the current from site 1 to site 2 or to site 4 or to the left lead regions. In particular, the operator for the current from site 2 to 1 and from site 4 to 1 can be identified as

$$\hat{I}_{2\to1} = \frac{ie}{\hbar}\left(e^{i\frac{\phi}{4}} c_2^\dagger c_1 - e^{-i\frac{\phi}{4}} c_1^\dagger c_2\right) \tag{4}$$

and

$$\hat{I}_{4\to1} = \frac{ie}{\hbar}\left(e^{-i\frac{\phi}{4}} c_4^\dagger c_1 - e^{i\frac{\phi}{4}} c_1^\dagger c_4\right), \tag{5}$$

whose averages give the bond currents flowing between sites 1 and 2 ($I_{2\to1}$) and 1 and 4 ($I_{4\to1}$). At steady state these two bond currents can be expressed as

$$I_{2\to1} = \frac{e}{\hbar}\int_{-\infty}^{+\infty} \frac{d\omega}{2\pi}\left[e^{i\frac{\phi}{4}} G_{12}^<(\omega) - e^{-i\frac{\phi}{4}} G_{21}^<(\omega)\right] \tag{6}$$

and

$$I_{4\to1} = \frac{e}{\hbar}\int_{-\infty}^{+\infty} \frac{d\omega}{2\pi}\left[e^{-i\frac{\phi}{4}} G_{14}^<(\omega) - e^{i\frac{\phi}{4}} G_{41}^<(\omega)\right], \tag{7}$$

where $G_{ab}^<$ is the ab matrix element of Fourier-transformed lesser projections of the system's Green's function to be introduced shortly. Note that these are the only independent bond currents flowing inside the molecule, as all other bond currents can be expressed in terms of these two currents due to stationarity of charge densities at all the sites in the molecule at steady state. Indeed, at steady state $I_{2\to5} = 0$, $I_{3\to2} = I_{2\to1}$, and $I_{3\to4} = I_{4\to1}$.

C. Net current in the circuit

The net current I_L (which is same as $-I_R$) flowing into the left lead from site 1 at steady state is given by the rate of change the average of charge on the left lead, i.e., $I_L(t) = \frac{d}{dt}(-e\sum_k \langle d^\dagger_{LK}(t) d_{LK}(t)\rangle)$. Similarly to the bond currents, the net current can also be expressed in terms of the system's greater and lesser Green's functions $G^{>/<}$ as [15]

$$I_L = \frac{e}{\hbar}\int_{-\infty}^{+\infty}\frac{d\omega}{2\pi}[\Sigma^<_{11}(\omega)G^>_{11}(\omega) - G^<_{11}(\omega)\Sigma^>_{11}(\omega)], \quad (8)$$

where $\Sigma^{>/<}$ are Fourier-transformed greater and lesser projections of contour-ordered self-energy to be introduced shortly. Note that the two terms on the right-hand side of Eq. (8) are real and represent inflow and outflow of the electrons from the left lead. On the other hand, such an interpretation is not possible for the two terms on the right-hand side of Eq. (6) and Eq. (7) as they are complex functions in general.

D. Green's function calculation

In order to calculate bond currents and net current in the circuit, we need to compute the system's Green's functions. These Green's functions (in matrix form) are defined on the Schwinger-Keldysh contour [15,16] as

$$G^c(\tau,\tau') = -\frac{i}{\hbar}\langle[\Theta(\tau,\tau')\Psi(\tau)\Psi^\dagger(\tau') - \Theta(\tau',\tau)\Psi^\dagger(\tau')^T\Psi(\tau)^T]\rangle, \quad (9)$$

where τ and τ' are contour times with

$$\Psi(\tau) = (c_1(\tau) \quad c_2(\tau) \quad c_3(\tau) \quad c_4(\tau) \quad c_5(\tau))^T \quad (10)$$

and $\Theta(\tau,\tau')$ is the Heaviside step function defined on the Schwinger-Keldysh contour [16]. $G^c(\tau,\tau')$ satisfies the following equation of motion [15,16]:

$$\int_c d\tau_1\left[\left(i\hbar\frac{\partial}{\partial\tau} - H_S\right)\delta^c(\tau,\tau_1) - \Sigma^c(\tau,\tau_1)\right]G^c(\tau_1,\tau') = \delta^c(\tau,\tau'), \quad (11)$$

where Σ^c is the self-energy due to interaction with the leads and has the following matrix structure:

$$\Sigma^c(\tau,\tau') = \begin{bmatrix} |g_L|^2\sum_{k,k'} G^0_{Lk,Lk'}(\tau,\tau') & 0 & 0 & 0 & 0 \\ 0 & 0 & 0 & 0 & 0 \\ 0 & 0 & |g_R|^2\sum_{k,k'} G^0_{Rk,Rk'}(\tau,\tau') & 0 & 0 \\ 0 & 0 & 0 & 0 & 0 \\ 0 & 0 & 0 & 0 & 0 \end{bmatrix}. \quad (12)$$

Here $G^0_{Lk,Lk'}(\tau,\tau')$ and $G^0_{Rk,Rk'}(\tau,\tau')$ are contour-ordered Green's functions for the isolated leads. Equation (11) can be projected onto the real times using Langreth rules to obtain all other real-time Green's functions [15]. At steady state all the Green's functions become time translational invariant and can be handled easily in the frequency domain. For example, the equation for the retarded system Green's function can be obtained from Eq. (11) by using Langreth rules and Fourier-transforming the resulting equation to get

$$[\omega I - H_0 - \Sigma^r(\omega)]G^r(\omega) = I, \quad (13)$$

where I is a 5×5 identity matrix and $\Sigma^r(\omega)$ is the Fourier-transformed retarded self-energy, obtained by Fourier-transforming the retarded projection of the contour-ordered self-energy $\Sigma^c(\tau,\tau')$ given in Eq. (12). The retarded Green's function can be obtained from the above equation by matrix inversion, i.e., $G^r(\omega) = [\omega I - H_0 - \Sigma^r(\omega)]^{-1}$. The advanced Green's function can be obtained in a similar manner, i.e., $G^a(\omega) = [\omega I - H_0 - \Sigma^a(\omega)]^{-1}$, where $\Sigma^a(\omega)$ is the Fourier-transformed advanced self-energy. Lesser and greater Green's functions can be obtained from

$$G^{</>}(\omega) = G^r(\omega)\Sigma^{</>}(\omega)G^a(\omega), \quad (14)$$

where $\Sigma^{</>}(\omega)$ are Fourier-transformed lesser and greater self-energies obtained by Fourier-transforming lesser and greater projections of the contour-ordered self-energy given in Eq. (12).

Thus obtained Green's functions can be used in Eqs. (6), (7), and (8) to get expressions for the bond currents, $I_{2\to1}$ and $I_{4\to1}$, and the net current, I_L, as (from here onwards we choose natural units such that $e = 1$, $c = 1$, and $\hbar = 1$)

$$I_{2\to1} = \int_{-\infty}^{+\infty}\frac{d\omega}{2\pi}\frac{\Gamma_L\Gamma_R[f_L(\omega) - f_R(\omega)]}{D[\omega]}\omega(\omega-\epsilon)\left[\{2\omega(\omega-\epsilon) - t^2\}\cos^2\left(\frac{\phi}{2}\right) + t^2\sin^2\left(\frac{\phi}{2}\right)\right]$$
$$+ \int_{-\infty}^{+\infty}\frac{d\omega}{2\pi}\frac{2[\Gamma_L f_L(\omega) + \Gamma_R f_R(\omega)]\sin(\phi)}{D[\omega]}(\omega-\epsilon)[\omega(\omega-\epsilon)(\omega^2-2) - t^2(\omega^2-1)], \quad (15)$$

$$I_{4\to1} = \int_{-\infty}^{+\infty} \frac{d\omega}{2\pi} \frac{\Gamma_L\Gamma_R[f_L(\omega) - f_R(\omega)]}{D[\omega]} \{\omega(\omega-\epsilon) - t^2\} \left[\{2\omega(\omega-\epsilon) - t^2\} \cos^2\left(\frac{\phi}{2}\right) - t^2 \sin^2\left(\frac{\phi}{2}\right) \right]$$
$$- \int_{-\infty}^{+\infty} \frac{d\omega}{2\pi} \frac{2[\Gamma_L f_L(\omega) + \Gamma_R f_R(\omega)] \sin(\phi)}{D[\omega]} (\omega-\epsilon)[\omega(\omega-\epsilon)(\omega^2-2) - t^2(\omega^2-1)], \tag{16}$$

and

$$I_L = \int_{-\infty}^{+\infty} \frac{d\omega}{2\pi} \frac{\Gamma_L\Gamma_R[f_L(\omega) - f_R(\omega)]}{D[\omega]} \left[\{2\omega(\omega-\epsilon) - t^2\}^2 \cos^2\left(\frac{\phi}{2}\right) + t^4 \sin^2\left(\frac{\phi}{2}\right) \right]. \tag{17}$$

Here $D[\omega] = [(\omega-\epsilon)\{\omega^4 - (\frac{\Gamma_L\Gamma_R}{4} + 4)\omega^2 + 4\sin^2(\frac{\phi}{2})\} - \omega t^2\{\omega^2 - 2 - \frac{\Gamma_L\Gamma_R}{4}\}]^2 + (\frac{\Gamma_L+\Gamma_R}{2})^2[\omega(\omega-\epsilon)(\omega^2-2) - t^2(\omega^2-1)]^2$, $\Gamma_\alpha = 2\pi\rho|g_\alpha|^2$, and $f_\alpha(\omega) = \frac{1}{e^{\beta_\alpha(\omega-\mu_\alpha)}+1}$. Here β_α and μ_α are, respectively the temperature and the chemical potential of the αth lead. From here onwards, we shall consider the case where temperatures of both the leads are the same ($\beta_L = \beta_R = \beta$). Note that Γ_L, Γ_R, β^{-1}, ϵ, t, and ω are dimensionless numbers given in units of the coupling between sites constituting the ring. Both the bond currents $I_{2\to1}$ and $I_{4\to1}$ have two contributions, one purely due to applied bias (and becomes zero for $eV = 0$) and the other purely due to applied magnetic flux (and becomes zero for $\phi = 0$). In passing, we note that $I_L = I_{2\to1} + I_{4\to1}$, which is nothing but Kirchoff's law. Notice that the net transmission function given as

$$T_L(\omega) = \frac{\Gamma_L\Gamma_R}{D[\omega]} \left[\{2\omega(\omega-\epsilon) - t^2\}^2 \cos^2\left(\frac{\phi}{2}\right) + t^4 \sin^2\left(\frac{\phi}{2}\right) \right] \tag{18}$$

has no real zeros (antiresonances) for $\phi \neq 2n\pi$ (n is any integer). For $\phi = 2n\pi$, $T_L(\omega)$ has zeros at $\omega = \frac{\epsilon \pm \sqrt{\epsilon^2+2t^2}}{2}$.

The two different cases, symmetric and asymmetric junctions, mentioned in the introduction, are special cases of the model presented in this section. They are obtained in the limits $t \to 0$ and $\phi \to 0$, respectively. We analyze these two cases separately in the next two sections.

Although we have chosen a symmetric gauge, where the dimensionless magnetic flux is equally distributed among all the bonds (just to show that the ring is symmetric), the expressions for the bond currents [Eq. (15) and Eq. (16)] and the net current [Eq. (17)] remain invariant under any gauge choice; hence the results are clearly gauge invariant. To be more specific an arbitrary gauge can be considered, where the single-particle Hamiltonian for the isolated molecule is

$$H_0 = \begin{bmatrix} 0 & -e^{-i\phi_{12}} & 0 & -e^{i\phi_{41}} & 0 \\ -e^{i\phi_{12}} & 0 & -e^{-i\phi_{23}} & 0 & -te^{-i\phi_{25}} \\ 0 & -e^{i\phi_{23}} & 0 & -e^{-i\phi_{34}} & 0 \\ -e^{-i\phi_{41}} & 0 & -e^{i\phi_{34}} & 0 & 0 \\ 0 & -te^{i\phi_{25}} & 0 & 0 & \epsilon \end{bmatrix} \tag{19}$$

such that $\phi_{12} + \phi_{23} + \phi_{34} + \phi_{41} = \phi$. By explicit calculation it can be shown that the expressions for the bond currents [Eq. (15) and Eq. (16)] and the net current [Eq. (17)] depend only on the sum of the phases (i.e., $\phi_{12} + \phi_{23} + \phi_{34} + \phi_{41} = \phi$); hence the results presented in this section do not depend on any specific gauge choice and the results are gauge invariant.

III. SYMMETRIC AHARONOV-BOHM RING

In this section we analyze the effect of applied magnetic field and bias on the bond currents flowing in a symmetric ring. We therefore take the limit of $t \to 0$ in the general equations (15), (16), and (17) given in Sec. II. The extra site (substituent) gets decoupled from the ring and hence does not affect the bond currents as well as the net current. The quantum Aharonov-Bohm effects on the net conductance of this junction is studied in Ref. [17], where the effects of magnetic flux and asymmetry between two branches on the net transmission function were analyzed. In this work we are mainly interested in controlling bond currents inside the molecule. For simplification we set $\Gamma_L = \Gamma_R = \Gamma$.

For this symmetric Aharonov-Bohm ring case, the bond currents become $I_{2\to1} = I_V + I_\phi$ and $I_{4\to1} = I_V - I_\phi$, where I_V and I_ϕ are given by

$$I_V = \int_{-\infty}^{+\infty} \frac{d\omega}{2\pi} \left[\frac{2\Gamma^2\omega^2 \cos^2(\frac{\phi}{2})}{D[\omega]} \right] [f_L(\omega) - f_R(\omega)] \tag{20}$$

and

$$I_\phi = \int_{-\infty}^{+\infty} \frac{d\omega}{2\pi} \left[\frac{2\Gamma\omega(\omega^2-2)\sin(\phi)}{D[\omega]} \right] [f_L(\omega) + f_R(\omega)] \tag{21}$$

with $D[\omega] = [\omega^4 - (\frac{\Gamma^2}{4} + 4)\omega^2 + 4\sin^2(\frac{\phi}{2})]^2 + \Gamma^2\omega^2[\omega^2 - 2]^2$. The expressions for $I_{2\to1}$ and $I_{4\to1}$ have two contributions: I_V is due to the applied chemical potential difference between two metallic leads and I_ϕ is the contribution driven due to the magnetic flux; this contribution vanishes only if ϕ is an integral multiple of 2π. Note that both the contributions vanish if ϕ is an odd integral multiple of π, irrespective of the applied bias. This behavior can be understood better if we analyze the bond current in the molecular eigenspace (Appendix A) and the net current in terms of spatial pathways (Appendix B). We find that the two contributions, I_ϕ and I_V, have different origins. Each eigenstate carries a current which depends on ϕ. These add up to give I_ϕ, while the I_V contribution comes due to the coherences induced by the leads between different eigenstates. I_V can also be interpreted as the net current due to two interfering pathways $1 \to 2 \to 3$ and $1 \to 4 \to 3$ in the molecule (Appendix B). At $\phi = \pi$, these two pathways interfere destructively and hence $I_V = 0$. On the other hand, $I_\phi = 0$ for $\phi = \pi$, as eigenstates which carry opposite currents become degenerate (Appendix A). When

$\phi = 0$ the bond current $I_{12} = I_V$; i.e., the contribution comes entirely from the coherences between eigenstates which cannot be described within the simplified Lindblad quantum master equation approach [18]. Analytical expressions for I_ϕ and I_V for both finite-temperature and zero-temperature cases are given in Appendix C. Note that for the bias-driven part, I_V, it is straightforward to define an energy-dependent transmission function $T(\omega) = [\frac{2\Gamma^2\omega^2\cos^2(\frac{\phi}{2})}{D[\omega]}]$; however the same is not possible for I_ϕ.

Close to equilibrium, by linearizing the two fluxes in ϕ and eV, we get

$$I_V = L_{VV} \times eV + L_{V\phi} \times \phi, \tag{22}$$

$$I_\phi = L_{\phi V} \times eV + L_{\phi\phi} \times \phi, \tag{23}$$

where $L_{VV} = \int_{-\infty}^{+\infty} \frac{d\omega}{2\pi}[\frac{2\Gamma^2\omega^2}{D[\omega]_{\phi=0}}]f'(\omega)$, $L_{\phi\phi} = \int_{-\infty}^{+\infty} \frac{d\omega}{2\pi}[\frac{4\Gamma\omega(\omega^2-2)}{D[\omega]_{\phi=0}}]f(\omega)$, and $L_{V\phi} = L_{\phi V} = 0$ are Onsager matrix elements. The off-diagonal elements are individually zero since (i) I_V is an even function of ϕ and $I_V = 0$ for $eV = 0$, hence the contribution linear in ϕ to I_V vanishes, and (ii) I_ϕ is an even function of eV (for $\mu = 0$) and $I_\phi = 0$ for ϕ, hence the contribution linear in eV to I_ϕ vanishes. Thus close to equilibrium the two fluxes, one originating from the applied bias and the other due to the applied magnetic field, are independent of each other. Therefore, close to equilibrium, the net current in the circuit ($2I_V$) cannot be manipulated by applied magnetic field. Note that here, ϕ acts as a thermodynamic force for the flux I_ϕ. This scenario is different from standard linear irreversible thermodynamics, where the cross Onsager matrix elements for a general case, where generalized fluxes J_m are driven by generalized forces X_n (i.e., $J_m = \sum_n L_{mn}X_n$), satisfy the Onsager-Casimir relationship [19] as a consequence of microscopic reversibility of underlying dynamics, $L_{mn}(\phi) = (-1)^{(\alpha_m+\alpha_n)}L_{nm}(-\phi)$ (α_m assumes 0 if J_m and X_m are symmetric under time reversal or 1 if J_m and X_m are antisymmetric under time reversal), where ϕ is treated as a parameter. Since here ϕ is an external force which drives I_ϕ, on time reversal both the force (ϕ) and hence the resultant flux (I_ϕ) change sign, which is consistent with linear irreversible thermodynamics [19].

A. Thermodynamic equilibrium

When $\mu_L = \mu_R = \mu$ and $\beta_L = \beta_R = \beta$, (i.e., when both the leads are at the same thermodynamic equilibrium) only the magnetic-field-driven current $I_\phi = I_{2\to1}$ exists ($I_{4\to1} = -I_{2\to1}$) and leads only act as phase breakers for the electronic motion in the molecular ring. Note that in this case ϕ may be arbitrarily large.

Figure 2 is a plot of the equilibrium bond current, I_ϕ, as a function of ϕ for various values of the chemical potential (μ) of leads at fixed Γ and β. It shows that at thermodynamic equilibrium, I_ϕ is a periodic function of ϕ with period 2π, although eigenstate energies, eigenstate contributions (to I_{phi}), and their populations are periodic in ϕ with period 8π. This is because the eigenstate populations and their respective contributions to I_ϕ get swapped after a 2π increase in ϕ such that I_ϕ remains periodic in ϕ with period 2π (Appendix A).

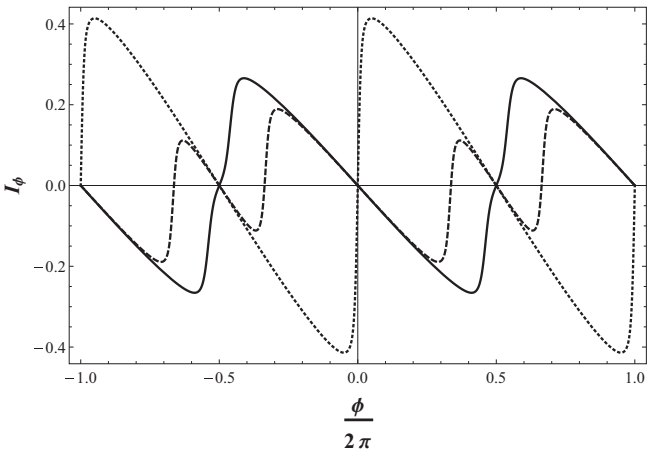

FIG. 2. Equilibrium bond current as a function of ϕ with $\Gamma = 0.1$ and $\beta = 100$. Here, dashed: $\mu = -1.0$, dotted: $\mu = 0$, and continuous: $\mu = 1.5$. Note that all energy values are given in units of coupling strength between sites constituting the ring.

We next analyze the effect of molecule-lead coupling on the equilibrium bond current. We note that the effect of molecule-lead coupling on the orbital magnetic moment density at equilibrium is studied in Ref. [20]. Figure 3 shows I_ϕ as a function of Γ at fixed μ and β for various values of ϕ. Increasing the coupling strength to leads, I_ϕ decreases because leads acts as phase breakers that hinder the coherent motion of electrons [21,22] and therefore suppresses the coherent current. As Γ is increased, different eigenstates mix strongly due to coupling to leads. This enhances scattering of electrons between different eigenstates and leads to dephasing. Said differently, the suppression of I_ϕ can also be understood as due to increasing overlap between density of states of different eigenstates carrying opposite currents, as Γ is increased. As $\Gamma \to \infty$ (specifically $\Gamma^2 \gg \Gamma\beta \gg 1$), I_ϕ decays to zero as

$$I_\phi \approx \frac{4\beta\sin(\phi)}{\pi^2\Gamma^2}\text{Re}\left[\Psi^{(1)}\left(\frac{1}{2} - \frac{i\beta\mu}{2\pi}\right)\right], \tag{24}$$

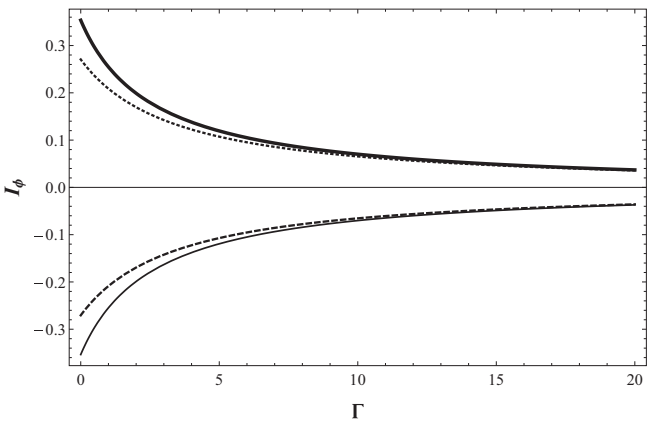

FIG. 3. Equilibrium bond current as a function of Γ with bare chemical potential $\mu = 0$ and $\beta = 100$. Here, dashed: $\phi = -\frac{\pi}{2}$, thin: $\phi = -\frac{\pi}{3}$, thick: $\phi = \frac{\pi}{3}$, and dotted: $\phi = \frac{\pi}{2}$.

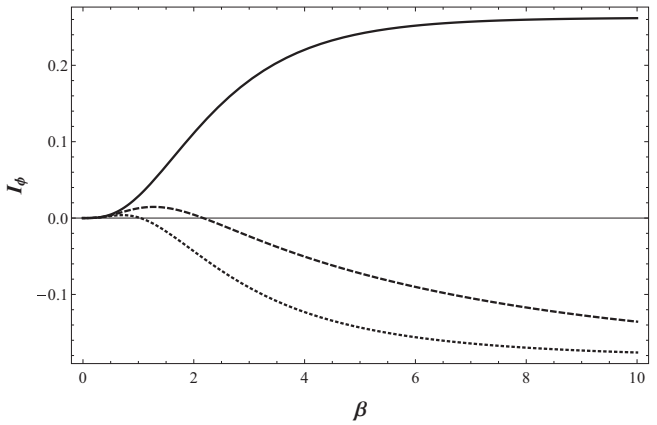

FIG. 4. Equilibrium bond current as a function of β with $\Gamma = 0.1$ and $\phi = \frac{\pi}{2}$. Here, dashed: $\mu = -1.0$, continuous: $\mu = 0$, and dotted: $\mu = 1.5$.

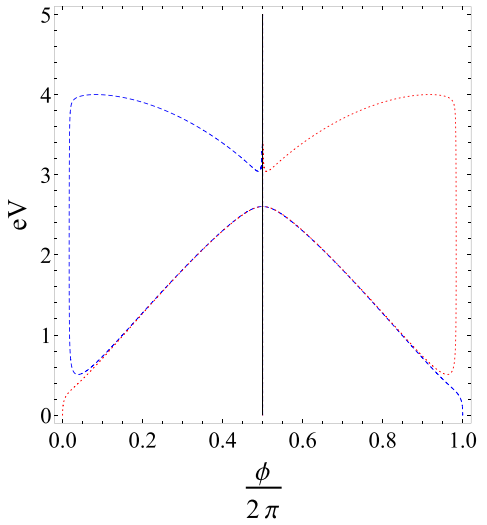

FIG. 5. Phase diagram for bond currents in the molecular ring. The two curves (red dotted and blue dashed) separate regions where both the branches are conducting and black line represents a region where both the branches are nonconducting. On the blue (dashed) curve only the lower branch is conducting, while on the red (dotted) curve the upper branch is conducting. Parameters chosen are $\Gamma = 0.1$, $\beta = 100$, $\mu = 0$, $\mu_L = \mu + eV/2$, and $\mu_R = \mu - eV/2$.

where $\Psi^{(1)}[Z]$ is the trigamma function [23] in variable Z. On the other hand, as $\Gamma \to 0$, I_ϕ reduces to the limit of circulating current in an isolated molecule which is given by the sum of the currents carried by eigenstates (Appendix A) multiplied by their respective populations (at thermodynamic equilibrium given by lead Fermi functions at the corresponding eigenstate energies).

As the temperature is increased, different eigenstates start to get populated due to coupling with leads. At high temperatures ($\beta \to 0$), the populations of various eigenstates become almost identical. As discussed in Appendix A, different eigenstates contribute oppositely to the current, and hence the net bond current diminishes as the temperature is increased. This is shown in Fig. 4. At small temperature ($\beta \to \infty$), the current approaches the sum of currents carried by all eigenstates with energies below μ (since only states below μ are occupied).

B. Out of thermodynamic equilibrium

We now consider the case when the two leads are not at the thermodynamic equilibrium, i.e., $\mu_L \neq \mu_R$ and $\beta_L = \beta_R = \beta$. Further, we take $\mu_L = \mu + \frac{eV}{2}$ and $\mu_R = \mu - \frac{eV}{2}$, with bare chemical potentials of the leads set in resonance with ring site energies ($\mu = 0$). In this case, the external bias also contributes to the bond currents and we have to consider both I_ϕ and I_V, given in Eqs. (20) and (21). We note that I_V is an even (odd) function of ϕ (eV), whereas I_ϕ is an odd (even) function of ϕ (eV). Hence, by changing the polarity of either eV or ϕ, it would be possible to make the two contributing currents flow in opposite directions leading to enhancement of current flowing along one branch and reduction of current flowing along the other branch. This is a trivial case. However we find that at finite bias (eV), ϕ can be tuned (without changing polarity) such that only one of the branches is conducting. This is shown in Fig. 5, where the white region in ϕ-eV space indicates that both the branches are conducting, the blue (dashed) curve corresponds to ϕ and eV values where only the lower branch is conducting ($I_{2\to1} = 0$), and the red (dotted) curve corresponds to ϕ and eV values where only the upper branch is conducting ($I_{4\to1} = 0$). It should be recalled that at $\phi = \pi$, due to destructive interference, both the branches are nonconducting and hence net current in the circuit is also zero (Appendix B), irrespective of the applied bias. This is indicated by a black line in the figure. Magnetic-field-driven (I_ϕ) and applied-bias-driven (I_V) contributions to the bond current are plotted in Fig. 6 as a function of ϕ and eV. Notice that I_ϕ changes sign with respect to both ϕ and eV, while direction of I_V cannot be changed by changing ϕ. The change in the sign of I_ϕ with ϕ is similar to the case discussed in the thermodynamic equilibrium. However the change in the sign of I_ϕ with eV happens because, as the bias increases, the populations of states with different contributions changes, resulting in sign change of I_ϕ. For large molecule-lead coupling strengths, I_ϕ goes to zero asymptotically (as $\approx \frac{1}{\Gamma^2}$) and hence circulating currents vanish.

The net current flowing in the circuit for the symmetric ($t = 0$) Aharonov-Bohm ring case becomes

$$I_L = \int_{-\infty}^{+\infty} \frac{d\omega}{2\pi} \left[\frac{4\Gamma^2 \omega^2 \cos^2\left(\frac{\phi}{2}\right)}{D[\omega]} \right] [f_L(\omega) - f_R(\omega)]. \quad (25)$$

Net current flowing in the circuit has been analyzed in several works to study the effects of the magnetic flux on the net current; for example, Refs. [7,17] studied the effect of magnetic field on net transmission function in an asymmetric ring system. In Ref. [24] the effect of inhomogeneous magnetic flux on the net current is analyzed. In Ref. [25] the effect of Coulomb interaction on the net current in the presence of magnetic flux is studied. Dissipation due to electron-phonon coupling and its effect on the net transmission has been studied in Ref. [26], and the effect of external electromagnetic field has been discussed in Ref. [27]. In the present work, since we are only interested in bond currents in the molecule, we do not pursue the net current further.

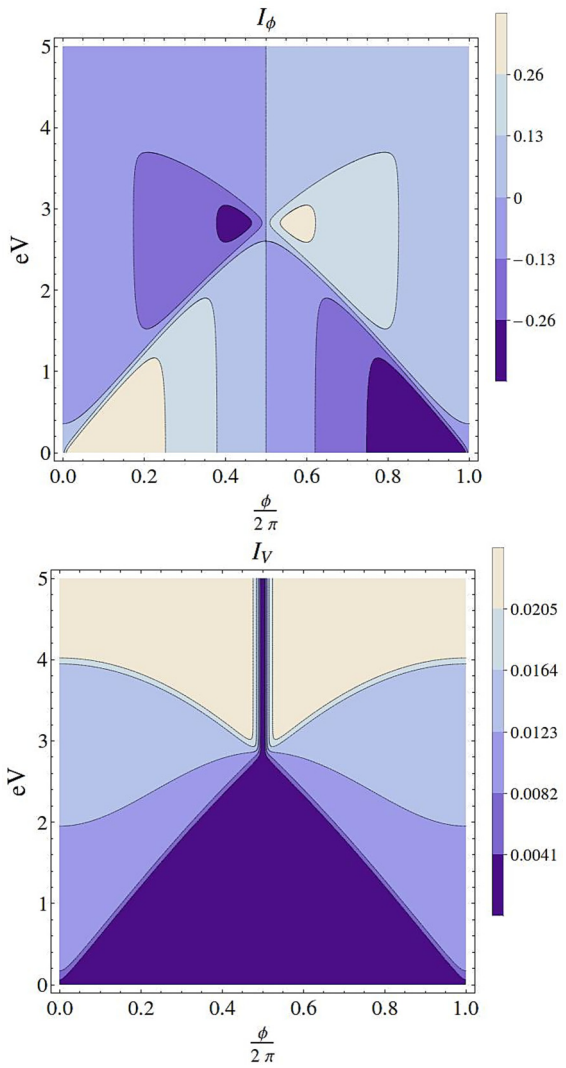

FIG. 6. Contributions, I_ϕ (upper panel) and I_V (lower panel), to bond currents are plotted as a function of ϕ and eV with $\Gamma = 0.1$, $\beta = 100$, $\mu = 0$, $\mu_L = \mu + eV/2$, and $\mu_R = \mu - eV/2$.

IV. EFFECT OF CHEMICAL SUBSTITUTION

Here we explore the effect of coupling an extra site (with site energy ϵ and coupling strength t) to an otherwise symmetric ring system. We analyze the effect of this substitution on the bond currents in the absence of magnetic field. The substitution introduces asymmetry between two paths that an electron can take in going from the left lead to the right lead. This leads to interference effects in the net current as discussed in Refs. [28,29]. However this asymmetry not only affects the net current but also the bond currents in the molecule and may lead to circulating currents (at finite bias) even in the absence of magnetic flux. The goal in this section is to study these circulating currents. To this end we take the limit $\phi \to 0$ of the general equations (15), (16), and (17), given in Sec. II. To further simplify the analysis, we consider the case $\Gamma_L = \Gamma_R = \Gamma$ and $\epsilon = 0$.

The expressions for the bond currents, $I_{2\to1}$ and $I_{4\to1}$, and the net current, I_L, assume the form

$$I_{2\to1} = \int_{-\infty}^{+\infty} \frac{d\omega}{2\pi}\left[\frac{\Gamma^2\omega^2(2\omega^2 - t^2)}{D[\omega]}\right][f_L(\omega) - f_R(\omega)], \tag{26}$$

$$I_{4\to1} = \int_{-\infty}^{+\infty} \frac{d\omega}{2\pi}\left[\frac{\Gamma^2(\omega^2-t^2)(2\omega^2-t^2)}{D[\omega]}\right][f_L(\omega)-f_R(\omega)], \tag{27}$$

$$I_L = \int_{-\infty}^{+\infty} \frac{d\omega}{2\pi}\left[\frac{\Gamma^2(2\omega^2 - t^2)^2}{D[\omega]}\right][f_L(\omega) - f_R(\omega)], \tag{28}$$

where $D[\omega] = \{\omega^2 + (\frac{\Gamma}{2})^2\}\{[(\omega^2 - t^2)(\omega^2 - 4) - 2t^2]^2 + (\frac{\Gamma}{2})^2\omega^2(\omega^2 - t^2)^2\}$. These currents are plotted as functions of eV and t in Fig. 7. Note that the bond current $I_{2\to1}$ (corresponding to the branch having the extra substituent) changes sign as bias is scanned, while $I_{4\to1}$ remains positive (in the direction of the net current).

Unlike the case in the presence of magnetic flux, in this case the two bond currents (which vanish at zero bias) have well-defined energy-dependent transmission functions, T_{12} and T_{14}. We note that both the transmission functions have common zeros at $\omega = \pm\frac{t}{\sqrt{2}}$. We analyze the nature of transmission functions at these zeros. Since $D[\omega = \pm\frac{t}{\sqrt{2}}] > 0$, it is clear that both T_{12} and T_{14} change sign in opposite directions around $\omega = \pm\frac{t}{\sqrt{2}}$. However the total transmission function, $T_L(\omega) = \frac{(2\omega^2-t^2)^2}{D[\omega]}$, attains its minimum value (zero) at these points (antiresonances). This behavior of bond transmission functions changing sign around antiresonances of the total transmission function was noticed by Jayannavar *et al.* [12], using scattering theory. Apart from the antiresonance points, T_{14} has extra zeros at $\omega = \pm t$, where it is an increasing (decreasing) function at $+t$ $(-t)$, and T_{12} has an extra zero at $\omega = 0$ where it has a maximum. For $|\omega| > t$, both $T_{12}(\omega)$ and $T_{14}(\omega)$ are positive functions of ω. Thus at energies $|\omega| > t$, the two bond currents flow in the same (positive) direction, while for $|\omega| < t$, the two currents flow in the opposite direction and a circulating current exists. The energy range $|\omega| < t$ is, therefore, critical for the existence of a circulating current in the molecule. Thus at low temperatures, the circulating current exists only for $|eV| < t$ (here $\mu = 0$ is assumed). In Fig. 8 we show a plot of $T_{12}(\omega)$, $T_{14}(\omega)$, and $T_L(\omega)$.

Zeros of transmission functions $T_{12}(\omega)$, $T_{14}(\omega)$, and $T_L(\omega)$ are analyzed using the projection operator method in Appendix D. The antiresonance (multipath zero) of $T_L(\omega)$ at $\omega = \pm\frac{t}{\sqrt{2}}$ is due to the destructive interference between two paths $1 \to 2 \to 3$ and $1 \to 4 \to 3$ that an electron can take through the molecule to go from left lead to right lead. This has been discussed before in Ref. [30]. The bond transmission functions, $T_{12}(\omega)$ and $T_{14}(\omega)$, have several zeros. The zero of $T_{12}(\omega)$ at $\omega = 0$ is due to the destructive interference between direct $(1 \to 2)$ and indirect $(1 \to 4 \to 3 \to 2)$ paths that an electron can take to go from site 1 to site 2 (note that for $\epsilon = 0$, this zero is degenerate, and it is also due to the energy of the electron being in resonance with the substituent site energy). Similarly, the zeros of $T_{14}(\omega)$ at $\omega = \pm t$ are due to the

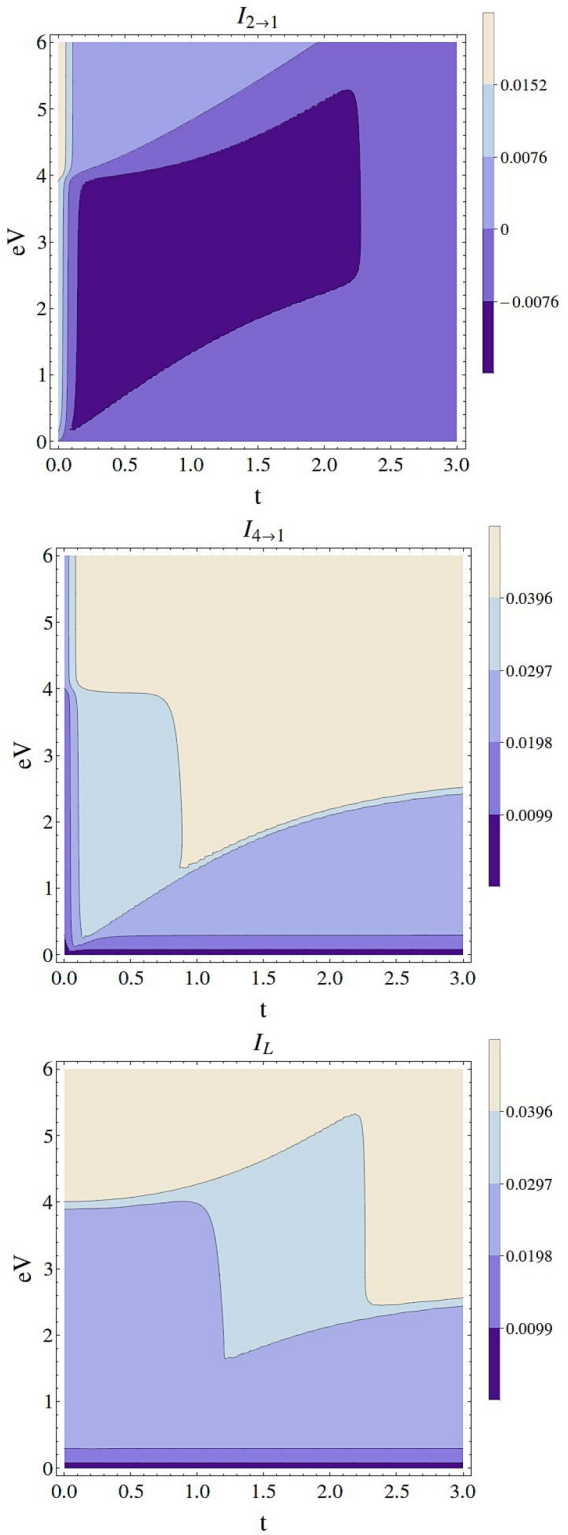

FIG. 7. Bond currents $I_{2\to1}$ and $I_{4\to1}$ together with the net current, I_L, as a function of t and eV with $\epsilon = 0$, $\Gamma = 0.1$, $\beta = 100$, $\mu = 0$, $\mu_L = \mu + eV/2$, and $\mu_R = \mu - eV/2$.

destructive interference between direct ($1 \to 4$) and indirect paths ($1 \to 2 \to 3 \to 4$). The bond transmission functions, $T_{12}(\omega)$ and $T_{14}(\omega)$, also have zeros at $\omega = \pm\frac{t}{\sqrt{2}}$, but they do not have a simple interpretation in this scheme.

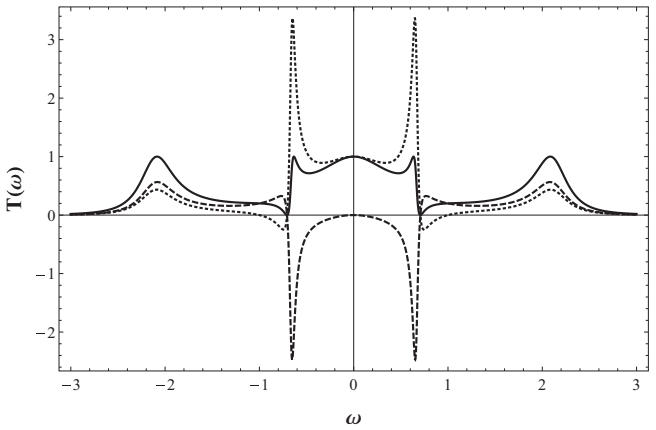

FIG. 8. Bond transmission functions T_{12} (dashed), T_{14} (dotted), and net transmission function T_L (continuous) as a function of ω with $\Gamma = 1$, $\epsilon = 0$, and $t = 1$.

As discussed earlier, the circulating current appears due to the negativity of I_{12} which comes from the negativity of T_{12} in the region $|\omega| < \frac{t}{\sqrt{2}}$, outside which T_{12} is positive. For $\Gamma \to \infty$ (specifically $\Gamma \gg t$), T_{12} in the region $|\omega| < \frac{t}{\sqrt{2}}$ goes to zero as $T_{12} \approx \frac{(2\omega^2 - t^2)}{(\omega^2 - t^2)^2} \frac{16}{\Gamma^2}$ and hence the negative contribution to $I_{2\to1}$ vanishes asymptotically. Therefore for large Γ, circulating current vanishes. Thus for sufficiently large bias (with $\mu = 0$), greater than $\frac{t}{\sqrt{2}}$, and at low temperatures it is therefore possible to change the sign of I_{12} (from negative to positive) by tuning the coupling strength, Γ (for high temperature this can happen even for $|eV| < \frac{t}{\sqrt{2}}$). Hence it is possible to switch between the phases with and without circulating currents in the molecule by tuning Γ. This is shown in Fig. 9, where the black region represents circulating current in the ring and the white region

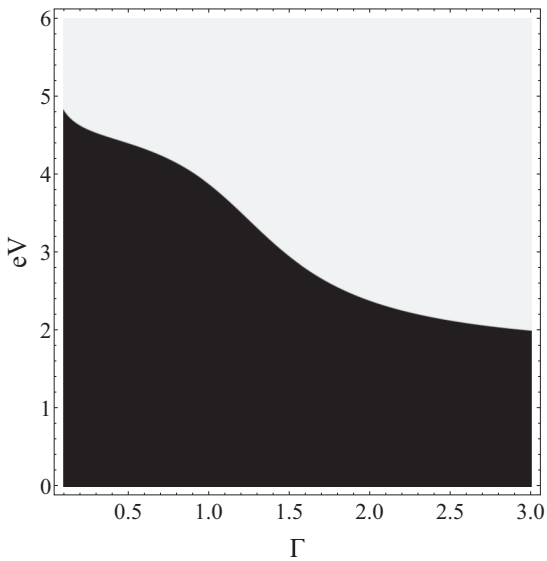

FIG. 9. Circulating current as a function of Γ and eV with $\mu_L = \mu + \frac{eV}{2}$, $\mu_R = \mu - \frac{eV}{2}$, $\mu = 0$, $\beta = 100$, $t = 1$, and $\epsilon = 0$. Here it is shown that switching between phases with circulating current (black region) and without circulating current (white region) can be done by tuning Γ for certain eV.

represents a region with no circulating current. It is clear that, for certain values of eV, it is possible to switch between phases with and without circulating current by changing Γ values. Note that T_{14} is also negative over a small energy window, $\frac{t}{\sqrt{2}} < |\omega| < t$, which is always compensated by the positive contribution from the region $|\omega| < \frac{t}{\sqrt{2}}$, leading to positive $I_{4\to1}$.

V. CONCLUSIONS

We have studied bond currents in a simple ring-shaped molecular junction in the presence of asymmetry and magnetic field. The first case studied is the symmetric Aharonov-Bohm ring coupled to metal leads, where we identified two contributions to bond currents, one induced by applied magnetic field (I_ϕ) and the other due to applied bias (I_V). These two contributions have different origins: the term I_ϕ is due to the population terms in the eigenstate basis and the term I_V is due to the coherences induced by leads between different eigenstates. It is possible to tune the applied bias and the applied magnetic field to completely suppress the current across one branch and enhance the current across the other branch. Lead-induced dephasing suppresses the circulating current which, for large lead couplings, dies off quadratically ($\approx\frac{1}{\Gamma^2}$). When an asymmetry is introduced by coupling a substituent on one of its branches, it is possible to generate a circulating current at finite bias, even in the absence of applied magnetic field by tuning the coupling strength of the substituent. Furthermore, we find that it is possible to switch between phases with and without circulating currents by tuning the coupling strength of the molecule with leads.

Although we have studied a specific simple model, so that analytical insights can be achieved, we feel that qualitative results do not change much under realistic conditions. To realize the proposed experiment with molecular junctions, using even relatively large molecules of typical dimensions $\sim$10 Å, is difficult as it needs unrealistically strong magnetic fields of strength $\sim$1000 T. Nevertheless, these results can be easily realized with artificial molecules (quantum dots) [31]. We note that an experiment has been carried out recently using magnetic fields of strength $\sim$1 T with a double quantum dot ring structure of radius $\sim$100 Å fabricated at the interface of semiconductor heterostructures (GaAs-AlGaAs) by applying gate potentials [32].

Here we have neglected the spin degree of freedom of the electrons. However, in the presence of the spin degree of freedom, the Zeeman splitting can be important and may qualitatively change the results presented in this paper. In the presence of the magnetic field, the single-particle electron states split into spin-up and spin-down states with linear shift in energy proportional to applied magnetic field strength. However in the presence of single-spin electrons, such a splitting can be neglected and the presented analysis strictly holds if spin-flip processes can be neglected on the system. This will be the case, for example, when ferromagnetic leads (both polarized in the same direction) are used instead of the normal-metal leads. The presented results also remain qualitatively valid when the Zeeman splitting energy scale is much smaller compared to the thermal energy scale, applied bias, and lead-induced broadening. Further, for large Zeeman splitting (large compared to the bias regime, lead-induced broadening, and thermal energies), as the spin-up (moves downward) and spin-down (moves upward) states move out of the applied-bias regime, one can suitably tune the external gate potential to bring one of the spin states into the conduction regime, and hence effectively the single-spin state would be important. Thus the theoretical scheme presented can be realized in experiments by choosing all energy scales in a controlled manner compared to the Zeeman scale for both small and large Zeeman splitting energies. But in the intermediate Zeeman splitting regime, where Zeeman splitting energy (linear in applied magnetic filed strength) is comparable to other energy scales, we expect to see few qualitative changes like some nonlinear modulations of both bond currents and net currents (due to linear dependence of site energies on applied magnetic field) superposed by the simple periodic trend expected in the small and large Zeeman splitting cases.

ACKNOWLEDGMENTS

H.Y. and U.H. acknowledge the financial support from the Indian Institute of Science (India).

APPENDIX A: EIGENSTATE PICTURE OF BOND CURRENTS IN SYMMETRIC AHARONOV-BOHM RING

The isolated molecule in the presence of magnetic flux is described by the Hamiltonian expressed in terms of Fock space operators,

$$\hat{H} = (c_1^\dagger \quad c_2^\dagger \quad c_3^\dagger \quad c_4^\dagger) H_{\text{system}} \begin{pmatrix} c_1 \\ c_2 \\ c_3 \\ c_4 \end{pmatrix} \tag{A1}$$

where H_{system} is the single-particle Hamiltonian for the symmetric ring system obtained by removing 5th row and 5th column from the matrix given in Eq. (2). The eigenstates of the single-particle Hamiltonian are given by

$$\psi_1 = \frac{1}{2}\begin{pmatrix} 1 \\ 1 \\ 1 \\ 1 \end{pmatrix}, \quad \psi_2 = \frac{1}{2}\begin{pmatrix} -i \\ -1 \\ i \\ 1 \end{pmatrix}, \quad \psi_3 = \frac{1}{2}\begin{pmatrix} i \\ -1 \\ -i \\ 1 \end{pmatrix},$$
$$\psi_4 = \frac{1}{2}\begin{pmatrix} -1 \\ 1 \\ -1 \\ 1 \end{pmatrix} \tag{A2}$$

with corresponding energies

$$\epsilon_1 = -2\cos\left(\frac{\phi}{4}\right), \quad \epsilon_2 = 2\sin\left(\frac{\phi}{4}\right), \quad \epsilon_3 = -2\sin\left(\frac{\phi}{4}\right),$$
$$\epsilon_4 = 2\cos\left(\frac{\phi}{4}\right), \tag{A3}$$

respectively. The Hamiltonian in the eigenbasis is expressed as

$$\hat{H} = \sum_{i=1}^{4} \epsilon_i A_i^\dagger A_i, \tag{A4}$$

where creation/annihilation ($A_i^\dagger A_i$) operators in the eigenbasis can be expressed in terms of creation/annihilation operators in the local basis as

$$\begin{pmatrix} A_1 \\ A_2 \\ A_3 \\ A_4 \end{pmatrix} = \mathcal{U}^\dagger \begin{pmatrix} c_1 \\ c_2 \\ c_3 \\ c_4 \end{pmatrix}, \tag{A5}$$

where matrix $\mathcal{U}$ has single-particle eigenstates given in Eq. (A2) as columns. Similarly, from Eqs. (4) and (5), $\hat{I}_{2\to1}$ and $\hat{I}_{4\to1}$ in the eigenbasis are given by

$$\hat{I}_{2\to1/4\to1} = \frac{i}{\hbar}(A_1^\dagger \quad A_2^\dagger \quad A_3^\dagger \quad A_4^\dagger) I_{\text{bond}_{2\to1/4\to1}} \begin{pmatrix} A_1 \\ A_2 \\ A_3 \\ A_4 \end{pmatrix}, \tag{A6}$$

where

$$I_{\text{bond}_{2\to1}} = \begin{pmatrix} \frac{1}{2}i\sin\left(\frac{\phi}{4}\right) & \left(\frac{1}{4}-\frac{i}{4}\right)\left[\sin\left(\frac{\phi}{4}\right)+\cos\left(\frac{\phi}{4}\right)\right] & \left(\frac{1}{4}+\frac{i}{4}\right)\left[\cos\left(\frac{\phi}{4}\right)-\sin\left(\frac{\phi}{4}\right)\right] & -\frac{1}{2}\cos\left(\frac{\phi}{4}\right) \\ \left(-\frac{1}{4}-\frac{i}{4}\right)\left[\sin\left(\frac{\phi}{4}\right)+\cos\left(\frac{\phi}{4}\right)\right] & \frac{1}{2}i\cos\left(\frac{\phi}{4}\right) & \frac{1}{2}\sin\left(\frac{\phi}{4}\right) & \left(\frac{1}{4}-\frac{i}{4}\right)\left[\cos\left(\frac{\phi}{4}\right)-\sin\left(\frac{\phi}{4}\right)\right] \\ \left(-\frac{1}{4}+\frac{i}{4}\right)\left[\cos\left(\frac{\phi}{4}\right)-\sin\left(\frac{\phi}{4}\right)\right] & -\frac{1}{2}\sin\left(\frac{\phi}{4}\right) & -\frac{1}{2}i\cos\left(\frac{\phi}{4}\right) & \left(\frac{1}{4}+\frac{i}{4}\right)\left[\sin\left(\frac{\phi}{4}\right)+\cos\left(\frac{\phi}{4}\right)\right] \\ \frac{1}{2}\cos\left(\frac{\phi}{4}\right) & \left(-\frac{1}{4}-\frac{i}{4}\right)\left[\cos\left(\frac{\phi}{4}\right)-\sin\left(\frac{\phi}{4}\right)\right] & \left(-\frac{1}{4}+\frac{i}{4}\right)\left[\sin\left(\frac{\phi}{4}\right)+\cos\left(\frac{\phi}{4}\right)\right] & -\frac{1}{2}i\sin\left(\frac{\phi}{4}\right) \end{pmatrix} \tag{A7}$$

and

$$I_{\text{bond}_{4\to1}} = \begin{pmatrix} -\frac{1}{2}i\sin\left(\frac{\phi}{4}\right) & \left(-\frac{1}{4}-\frac{i}{4}\right)\left[\cos\left(\frac{\phi}{4}\right)+\sin\left(\frac{\phi}{4}\right)\right] & \left(-\frac{1}{4}+\frac{i}{4}\right)\left[\cos\left(\frac{\phi}{4}\right)-\sin\left(\frac{\phi}{4}\right)\right] & -\frac{1}{2}\cos\left(\frac{\phi}{4}\right) \\ \left(\frac{1}{4}-\frac{i}{4}\right)\left[\cos\left(\frac{\phi}{4}\right)+\sin\left(\frac{\phi}{4}\right)\right] & -\frac{1}{2}i\cos\left(\frac{\phi}{4}\right) & \frac{1}{2}\sin\left(\frac{\phi}{4}\right) & \left(-\frac{1}{4}-\frac{i}{4}\right)\left[\cos\left(\frac{\phi}{4}\right)-\sin\left(\frac{\phi}{4}\right)\right] \\ \left(\frac{1}{4}+\frac{i}{4}\right)\left[\cos\left(\frac{\phi}{4}\right)-\sin\left(\frac{\phi}{4}\right)\right] & -\frac{1}{2}\sin\left(\frac{\phi}{4}\right) & \frac{1}{2}i\cos\left(\frac{\phi}{4}\right) & \left(-\frac{1}{4}+\frac{i}{4}\right)\left[\cos\left(\frac{\phi}{4}\right)+\sin\left(\frac{\phi}{4}\right)\right] \\ \frac{1}{2}\cos\left(\frac{\phi}{4}\right) & \left(\frac{1}{4}-\frac{i}{4}\right)\left[\cos\left(\frac{\phi}{4}\right)-\sin\left(\frac{\phi}{4}\right)\right] & \left(\frac{1}{4}+\frac{i}{4}\right)\left[\cos\left(\frac{\phi}{4}\right)+\sin\left(\frac{\phi}{4}\right)\right] & \frac{1}{2}i\sin\left(\frac{\phi}{4}\right) \end{pmatrix}. \tag{A8}$$

Here the diagonal elements of $I_{\text{bond}_{\alpha\to1}}$ multiplied by their respective populations give bond currents (between sites α and 1 for $\alpha = 2,4$) carried by different eigenstates.

It is clear that in the isolated molecule described by a thermal ensemble, only populations contribute to bond currents. But if the molecule is connected to leads, coherences can be induced between eigenstates and hence bond currents also change. It is clear that the eigenstate Lindblad master equation can give nonzero bond currents (as eigenstates themselves carry finite currents), albeit a wrong result out of equilibrium [18].

The lesser Green's function matrix, $G^<(\omega)$, can be transformed into the eigenbasis as $\tilde{G}^<(\omega) = \mathcal{U}^\dagger G^<(\omega)\mathcal{U}$. From this, the bond currents are calculated using $I_{\alpha\to1} = \int_{-\infty}^{+\infty} \frac{d\omega}{2\pi} \text{Tr}[I_{\text{bond}_{\alpha\to1}} \tilde{G}^<(\omega)]$ for $\alpha = 2,4$. By explicit calculation it can be seen (for the case $\Gamma_L = \Gamma_R = \Gamma$) that $I_{2\to1} = I_V + I_\phi$ and $I_{4\to1} = I_V - I_\phi$, where only population terms of $\tilde{G}^<(\omega)$ contribute to I_ϕ and coherences contribute to I_V.

For thermodynamic equilibrium (i.e., $\mu_L = \mu_R = \mu$ and $\beta_L = \beta_R = \beta$), eigenstate energies, eigenstate populations $[-i\int_{-\infty}^{+\infty} \frac{d\omega}{2\pi} G^<_{mm}(\omega)]$, and eigenstate contributions to I_ϕ are periodic in ϕ with period 8π as shown in Figs. 10, 11, and 12. The net contribution of each eigenstate is also periodic in ϕ with period 8π as shown in Fig. 13, but I_ϕ is periodic in ϕ with period 2π as can be seen in Fig. 14. This is because eigenstate energies, eigenstate contributions ($I_{\text{bond}_{2\to1_{mm}}}$) to I_ϕ, and eigenstate populations get swapped after a 2π increment in ϕ as can be seen in Figs. 10, 11, and 12. Furthermore, for $\phi = \pi$, states with opposite contributions to current I_ϕ become degenerate, hence the circulating current vanishes. Note that the difference in Fig. 2 and Fig. 14 is solely due to the temperature difference which affects the populations of the

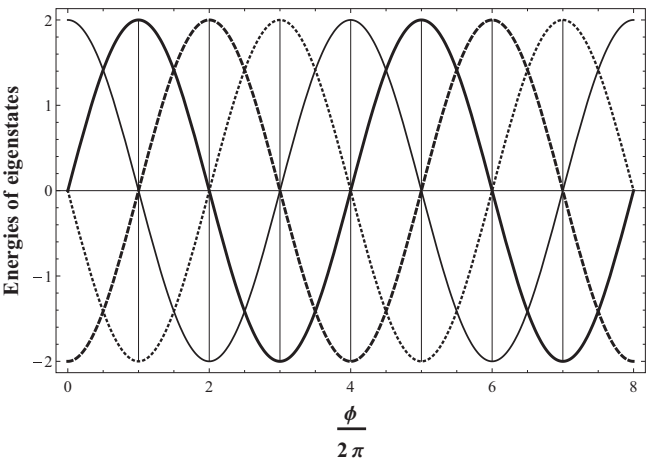

FIG. 10. Eigenvalues of isolated ring as a function of ϕ. Dashed, thick, dotted, and thin curves represent eigenstate energies of states 1, 2, 3, and 4.

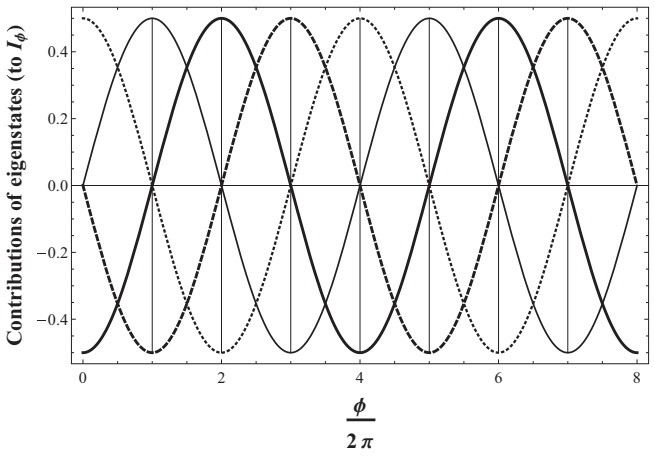

FIG. 11. Contribution of various eigenstates to I_ϕ as a function of ϕ. Dashed, thick, dotted, and thin curves represent contribution of eigenstates 1, 2, 3, and 4 to I_ϕ.

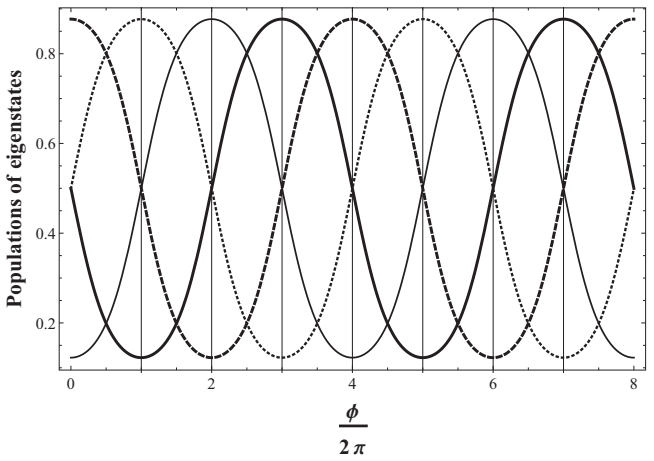

FIG. 12. Populations of various eigenstates of ring connected to reservoir as a function of ϕ with $\mu = 0$, $eV = 0$, $\beta = 1$, and $\Gamma = 0.1$. Dashed, thick, dotted, and thin curves represent populations of eigenstates 1, 2, 3, and 4.

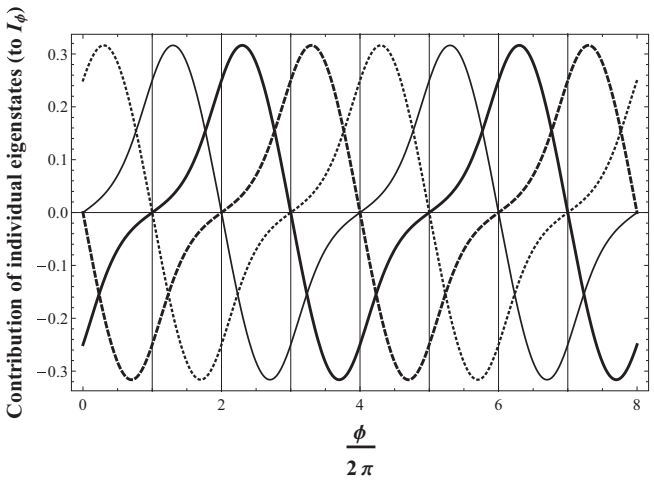

FIG. 13. Individual contributions of eigenstates as a function of ϕ with $\mu = 0$, $eV = 0$, $\beta = 1$, and $\Gamma = 0.1$. Dashed, thick, dotted, and thin curves represent individual contributions of eigenstates 1, 2, 3, and 4 to I_ϕ.

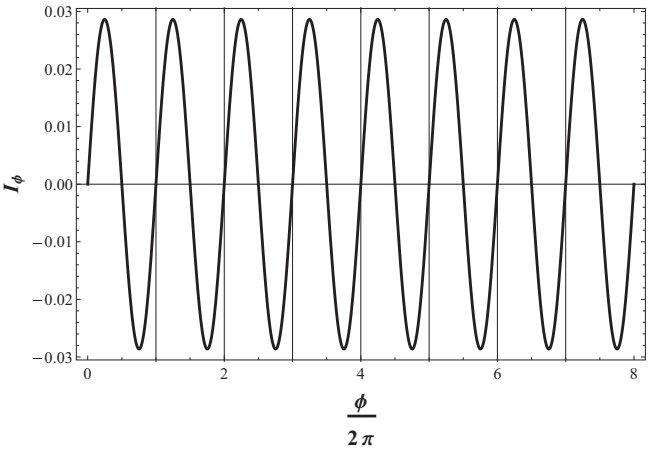

FIG. 14. I_ϕ as a function of ϕ with $\mu = 0$, $eV = 0$, $\beta = 1$, and $\Gamma = 0.1$.

eigenstates in the molecule. At low temperatures (as $\beta = 100$ in Fig. 2), as the magnetic field is varied, there will be a sharp change in the populations of states which contribute differently to bond currents, as the states which lie below the chemical potential change as a function of magnetic flux. But at high temperatures (as $\beta = 1$ in Fig. 14), the population changes are smooth, due to large thermal energy. Thus the changes in the bond current as a function of applied magnetic flux are also smooth.

APPENDIX B: SPATIAL PATH PICTURE OF NET CURRENT IN SYMMETRIC AHARONOV-BOHM RING

For noninteracting electron systems considered here, the net current in the circuit [which can be obtained by using Eq. (14) in Eq. (8)] can be expressed as

$$I_L = \int_{-\infty}^{+\infty} \frac{d\omega}{2\pi} \left[\Gamma_L G^r_{13}(\omega)\Gamma_R G^a_{31}(\omega)\right][f_L(\omega) - f_R(\omega)]. \tag{B1}$$

Following Ref. [30], we use the projection operator technique to project out sites 2 and 4 and obtain

$$G^r_{13}(\omega) = \frac{1}{\omega + i\frac{\Gamma_L}{2} - \Sigma^U_{11} - \Sigma^L_{11} - \frac{\left(\Sigma^U_{13}+\Sigma^L_{13}\right)\left(\Sigma^U_{31}+\Sigma^L_{31}\right)}{\omega + i\frac{\Gamma_R}{2} - \Sigma^U_{33} - \Sigma^L_{33}}} \times \left(\Sigma^U_{13} + \Sigma^L_{13}\right) \times \frac{1}{\omega + i\frac{\Gamma_R}{2} - \Sigma^U_{33} - \Sigma^L_{33}}. \tag{B2}$$

The first term in the product corresponds to the renormalized retarded Green's function for site 1 with self-energies coming from excursions into the upper branch (Σ^U_{11}), lower branch (Σ^L_{11}), and to and fro excursions to site 3 ($\frac{(\Sigma^U_{13}+\Sigma^L_{13})(\Sigma^U_{31}+\Sigma^L_{31})}{\omega + i\frac{\Gamma_R}{2} - \Sigma^U_{33} - \Sigma^L_{33}}$). The second term corresponds to the sum of bare amplitudes to go from site 1 to site 3 through upper (Σ^U_{13}) and lower branches (Σ^L_{13}). The third term corresponds to the retarded Green's function for site 3 with self-energies coming from excursions into the upper branch (Σ^U_{33}) and lower branch (Σ^L_{33}) only. $\Sigma^{U/L}_{ab}$ are matrix elements of self-energies due to upper/lower branches, respectively, and they are given by $\Sigma^U =$

$\frac{1}{\omega}\begin{pmatrix}1 & e^{i\frac{\phi}{2}}\\ e^{-i\frac{\phi}{2}} & 1\end{pmatrix}$ and $\Sigma^L = \frac{1}{\omega}\begin{pmatrix}1 & e^{-i\frac{\phi}{2}}\\ e^{i\frac{\phi}{2}} & 1\end{pmatrix}$. $G^a_{31}(\omega)$ can be obtained as $G^a_{31}(\omega) = [G^r_{13}(\omega)]^*|_{\phi\to-\phi}$. For $\phi = \pi$, the two pathways $1 \to 2 \to 3$ and $1 \to 4 \to 3$ destructively interfere [since $(\Sigma^U_{13} + \Sigma^L_{13})|_{\phi=\pi} = (\frac{e^{i\frac{\phi}{2}}}{\omega} + \frac{e^{-i\frac{\phi}{2}}}{\omega})|_{\phi=\pi} = 0$] leading to zero net current in the circuit. Also for $\phi \neq 2n\pi$ (n is any integer), the net transmission function $T_L(\omega) = \Gamma_L G^r_{13}(\omega)\Gamma_R G^a_{31}(\omega)$ has a zero (antiresonance) at $\omega = 0$, which is a resonance zero [30] (since the particle injected from the lead into the system at this energy is in resonance with sites 2 and 4).

APPENDIX C: ANALYTICAL EXPRESSIONS FOR CURRENTS FOR THE SYMMETRIC AHARONOV-BOHM RING

1. Finite-temperature expressions

The frequency integrals in Eqs. (20) and (21) can be performed using contour integration technique to get

$$\begin{aligned}
I_V = \frac{\Gamma^2\cos^2(\frac{\phi}{2})}{2\pi}\Bigg[&\frac{ia_1}{(a_1^2-a_2^2)(a_1^2-a_3^2)(a_1^2-a_4^2)}\Bigg\{\Psi\left[\frac{1}{2}-i\frac{\beta}{2\pi}(\mu_L+ia_1)\right]-\Psi\left[\frac{1}{2}+i\frac{\beta}{2\pi}(\mu_L-ia_1)\right]\\
&+\Psi\left[\frac{1}{2}+i\frac{\beta}{2\pi}(\mu_R-ia_1)\right]-\Psi\left[\frac{1}{2}-i\frac{\beta}{2\pi}(\mu_R+ia_1)\right]\Bigg\}\\
&+\frac{ia_2}{(a_2^2-a_1^2)(a_2^2-a_3^2)(a_2^2-a_4^2)}\Bigg\{\Psi\left[\frac{1}{2}-i\frac{\beta}{2\pi}(\mu_L+ia_2)\right]-\Psi\left[\frac{1}{2}+i\frac{\beta}{2\pi}(\mu_L-ia_2)\right]\\
&+\Psi\left[\frac{1}{2}+i\frac{\beta}{2\pi}(\mu_R-ia_2)\right]-\Psi\left[\frac{1}{2}-i\frac{\beta}{2\pi}(\mu_R+ia_2)\right]\Bigg\}\\
&+\frac{ia_3}{(a_3^2-a_1^2)(a_3^2-a_2^2)(a_3^2-a_4^2)}\Bigg\{\Psi\left[\frac{1}{2}-i\frac{\beta}{2\pi}(\mu_L+ia_3)\right]-\Psi\left[\frac{1}{2}+i\frac{\beta}{2\pi}(\mu_L-ia_3)\right]\\
&+\Psi\left[\frac{1}{2}+i\frac{\beta}{2\pi}(\mu_R-ia_3)\right]-\Psi\left[\frac{1}{2}-i\frac{\beta}{2\pi}(\mu_R+ia_3)\right]\Bigg\}\\
&+\frac{ia_4}{(a_4^2-a_1^2)(a_4^2-a_2^2)(a_4^2-a_3^2)}\Bigg\{\Psi\left[\frac{1}{2}-i\frac{\beta}{2\pi}(\mu_L+ia_4)\right]-\Psi\left[\frac{1}{2}+i\frac{\beta}{2\pi}(\mu_L-ia_4)\right]\\
&+\Psi\left[\frac{1}{2}+i\frac{\beta}{2\pi}(\mu_R-ia_4)\right]-\Psi\left[\frac{1}{2}-i\frac{\beta}{2\pi}(\mu_R+ia_4)\right]\Bigg\}\Bigg]
\end{aligned} \tag{C1}$$

and

$$\begin{aligned}
I_\phi = \frac{\Gamma\sin(\phi)}{2\pi}\Bigg[&\frac{a_1^2+2}{(a_1^2-a_2^2)(a_1^2-a_3^2)(a_1^2-a_4^2)}\Bigg\{\Psi\left[\frac{1}{2}+i\frac{\beta}{2\pi}(\mu_L-ia_1)\right]+\Psi\left[\frac{1}{2}-i\frac{\beta}{2\pi}(\mu_L+ia_1)\right]\\
&+\Psi\left[\frac{1}{2}+i\frac{\beta}{2\pi}(\mu_R-ia_1)\right]+\Psi\left[\frac{1}{2}-i\frac{\beta}{2\pi}(\mu_R+ia_1)\right]\Bigg\}\\
&+\frac{a_2^2+2}{(a_2^2-a_1^2)(a_2^2-a_3^2)(a_2^2-a_4^2)}\Bigg\{\Psi\left[\frac{1}{2}+i\frac{\beta}{2\pi}(\mu_L-ia_2)\right]+\Psi\left[\frac{1}{2}-i\frac{\beta}{2\pi}(\mu_L+ia_2)\right]\\
&+\Psi\left[\frac{1}{2}+i\frac{\beta}{2\pi}(\mu_R-ia_2)\right]+\Psi\left[\frac{1}{2}-i\frac{\beta}{2\pi}(\mu_R+ia_2)\right]\Bigg\}\\
&+\frac{a_3^2+2}{(a_3^2-a_1^2)(a_3^2-a_2^2)(a_3^2-a_4^2)}\Bigg\{\Bigg[\frac{1}{2}+i\frac{\beta}{2\pi}(\mu_L-ia_3)\Bigg]+\Psi\left[\frac{1}{2}-i\frac{\beta}{2\pi}(\mu_L+ia_3)\right]\\
&+\Psi\left[\frac{1}{2}+i\frac{\beta}{2\pi}(\mu_R-ia_3)\right]+\Psi\left[\frac{1}{2}-i\frac{\beta}{2\pi}(\mu_R+ia_3)\right]\Bigg\}\\
&+\frac{a_4^2+2}{(a_4^2-a_1^2)(a_4^2-a_2^2)(a_4^2-a_3^2)}\Bigg\{\Psi\left[\frac{1}{2}+i\frac{\beta}{2\pi}(\mu_L-ia_4)\right]+\Psi\left[\frac{1}{2}-i\frac{\beta}{2\pi}(\mu_L+ia_4)\right]\\
&+\Psi\left[\frac{1}{2}+i\frac{\beta}{2\pi}(\mu_R-ia_4)\right]+\Psi\left[\frac{1}{2}-i\frac{\beta}{2\pi}(\mu_R+ia_4)\right]\Bigg\}\Bigg],
\end{aligned} \tag{C2}$$

where $a_1 = \frac{\Gamma+\sqrt{\Gamma^2-64\sin^2(\frac{\phi}{4})}}{4}$, $a_2 = \frac{\Gamma-\sqrt{\Gamma^2-64\sin^2(\frac{\phi}{4})}}{4}$, $a_3 = \frac{\Gamma+\sqrt{\Gamma^2-64\cos^2(\frac{\phi}{4})}}{4}$, $a_4 = \frac{\Gamma-\sqrt{\Gamma^2-64\cos^2(\frac{\phi}{4})}}{4}$ and $\Psi[z]$ is digamma function in variable z [23].

2. Zero-temperature expressions

The frequency integrals can be performed after taking zero-temperature ($\beta \to \infty$) limits in Eqs. (20) and (21) to get

$$\begin{aligned} I_V = 2\Gamma^2 \cos^2\left(\frac{\phi}{2}\right)\Bigg\{ & \frac{a_1}{(a_1^2-a_2^2)(a_1^2-a_3^2)(a_1^2-a_4^2)}\left[\arctan\left(\frac{\mu_L}{a_1}\right)-\arctan\left(\frac{\mu_R}{a_1}\right)\right] \\ & + \frac{a_2}{(a_2^2-a_1^2)(a_2^2-a_3^2)(a_2^2-a_4^2)}\left[\arctan\left(\frac{\mu_L}{a_2}\right)-\arctan\left(\frac{\mu_R}{a_2}\right)\right] \\ & + \frac{a_3}{(a_3^2-a_1^2)(a_3^2-a_2^2)(a_3^2-a_4^2)}\left[\arctan\left(\frac{\mu_L}{a_3}\right)-\arctan\left(\frac{\mu_R}{a_3}\right)\right] \\ & + \frac{a_4}{(a_4^2-a_1^2)(a_4^2-a_2^2)(a_4^2-a_3^2)}\left[\arctan\left(\frac{\mu_L}{a_4}\right)-\arctan\left(\frac{\mu_R}{a_4}\right)\right]\Bigg\} \end{aligned} \tag{C3}$$

and

$$\begin{aligned} I_\phi = 2\Gamma \sin(\phi)\Bigg\{ & \frac{a_1^2+2}{(a_1^2-a_2^2)(a_1^2-a_3^2)(a_1^2-a_4^2)}\left[\ln(\mu_L^2+a_1^2)+\ln(\mu_R^2+a_1^2)\right] \\ & + \frac{a_2^2+2}{(a_2^2-a_1^2)(a_2^2-a_3^2)(a_2^2-a_4^2)}\left[\ln(\mu_L^2+a_2^2)+\ln\left(\mu_R^2+a_2^2\right)\right] \\ & + \frac{a_3^2+2}{(a_3^2-a_1^2)(a_3^2-a_2^2)(a_3^2-a_4^2)}\left[\ln(\mu_L^2+a_3^2)+\ln\left(\mu_R^2+a_3^2\right)\right] \\ & + \frac{a_4^2+2}{(a_4^2-a_1^2)(a_4^2-a_2^2)(a_4^2-a_3^2)}\left[\ln(\mu_L^2+a_4^2)+\ln\left(\mu_R^2+a_4^2\right)\right]\Bigg\}. \end{aligned} \tag{C4}$$

APPENDIX D: INTERPRETATION OF ZEROS OF TRANSMISSION FUNCTIONS FOR ASYMMETRIC RING JUNCTION

Here we analyze the zeros of the transmission functions for the $\epsilon \neq 0$ case. The $\epsilon = 0$ case discussed in the main text can be obtained trivially. Using Eq. (14) in Eq. (8), the net current in the circuit can be recast as

$$I_L = \int_{-\infty}^{+\infty} \frac{d\omega}{2\pi}\left[\Gamma_L G^r_{13}(\omega)\Gamma_R G^a_{31}(\omega)\right][f_L(\omega)-f_R(\omega)]. \tag{D1}$$

Similarly to Appendix B, we project out sites 2, 4, and 5 to obtain expression for $G^r_{13}(\omega)$ as

$$\begin{aligned} G^r_{13}(\omega) = & \frac{1}{\omega + i\frac{\Gamma_L}{2} - \Sigma^U_{11} - \Sigma^L_{11} - \frac{\left(\Sigma^U_{13}+\Sigma^L_{13}\right)\left(\Sigma^U_{31}+\Sigma^L_{31}\right)}{\omega + i\frac{\Gamma_R}{2} - \Sigma^U_{33} - \Sigma^L_{33}}} \\ & \times \left(\Sigma^U_{13}+\Sigma^L_{13}\right) \times \frac{1}{\omega + i\frac{\Gamma_R}{2} - \Sigma^U_{33} - \Sigma^L_{33}}. \end{aligned} \tag{D2}$$

The interpretation of three terms in $G^a_{13}(\omega)$ is the same as discussed in Appendix B. $\Sigma^{U/L}_{ab}$ are matrix elements of self-energies due to upper/lower branch; they are given by $\Sigma^U = \frac{(\omega-\epsilon)}{\omega(\omega-\epsilon)-t^2}\begin{pmatrix}1 & 1\\ 1 & 1\end{pmatrix}$ and $\Sigma^L = \frac{1}{\omega}\begin{pmatrix}1 & 1\\ 1 & 1\end{pmatrix}$. $G^a_{31}(\omega)$ can be obtained as $G^a_{31}(\omega) = [G^r_{13}(\omega)]^*$. For $\omega = \frac{\epsilon \pm \sqrt{\epsilon^2+2t^2}}{2}$, the two pathways $1 \to 2 \to 3$ and $1 \to 4 \to 3$ destructively interfere [since $(\Sigma^U_{13}+\Sigma^L_{13})|_{\omega = \frac{\epsilon \pm \sqrt{\epsilon^2+2t^2}}{2}} = 0$] leading to zeros (antiresonances termed as multipath zeros [30]) in the net transmission coefficient (this is due to the destructive interference between the upper and lower branch to go from site 1 to site 3, as the individual amplitudes are nonzero). However in the presence of applied magnetic field, these antiresonances in $T_L(\omega)$ disappear [Eq. (18)].

Using Eq. (14) in Eqs. (6) and (7) (additionally using $\mathrm{Im}[G^r_{13}(\omega)G^a_{32}(\omega)] = -\mathrm{Im}[G^r_{11}(\omega)G^a_{12}(\omega)]$ and $\mathrm{Im}[G^r_{13}(\omega)G^a_{34}(\omega)] = -\mathrm{Im}[G^r_{11}(\omega)G^a_{14}(\omega)]$ for $\phi = 0$ case), expressions for the two bond currents $I_{2\to1}$ and $I_{4\to1}$, given by Eqs. (6) and (7) with $\phi = 0$ and $\Gamma_L = \Gamma_R = \Gamma$, can be cast as

$$I_{2\to1} = -2\int_{-\infty}^{+\infty} \frac{d\omega}{2\pi}\Gamma\,\mathrm{Im}\left[G^r_{11}(\omega)G^a_{12}(\omega)\right][f_L(\omega)-f_R(\omega)], \tag{D3}$$

$$I_{4\to1} = -2\int_{-\infty}^{+\infty} \frac{d\omega}{2\pi}\Gamma\,\mathrm{Im}\left[G^r_{11}(\omega)G^a_{14}(\omega)\right][f_L(\omega)-f_R(\omega)]. \tag{D4}$$

To analyze zeros of the transmission function $T_{12}(\omega) = -2\Gamma\,\mathrm{Im}[G^r_{11}(\omega)G^a_{12}(\omega)]$, for the current between sites 1 and 2, we follow the same procedure as above and project out sites 3, 4, and 5 to get

$$G^r_{11}(\omega) = \frac{1}{\omega + i\frac{\Gamma}{2} - \Sigma^I_{11} - \frac{\left(\Sigma^D_{12}+\Sigma^I_{12}\right)\left(\Sigma^D_{21}+\Sigma^I_{21}\right)}{\omega - \Sigma^I_{22} - \Sigma^S_{22}}} \tag{D5}$$

and

$$G^a_{12}(\omega) = \frac{1}{\omega - i\frac{\Gamma}{2} - \left(\Sigma^I_{11}\right)^* - \frac{\left[\left(\Sigma^D_{12}\right)^* + \left(\Sigma^I_{12}\right)^*\right]\left[\left(\Sigma^D_{21}\right)^* + \left(\Sigma^I_{21}\right)^*\right]}{\omega - \left(\Sigma^I_{22}\right)^* - \left(\Sigma^S_{22}\right)^*}} \times \left[\left(\Sigma^D_{12}\right)^* + \left(\Sigma^I_{12}\right)^*\right] \times \frac{1}{\omega - \left(\Sigma^I_{22}\right)^* - \left(\Sigma^S_{22}\right)^*}. \tag{D6}$$

$\Sigma^{D(I)}_{ab}$ are matrix elements of self-energies due to direct path $1 \to 2$ (indirect path $1 \to 4 \to 3 \to 2$) given by $\Sigma^D = \begin{pmatrix} 0 & -1 \\ -1 & 0 \end{pmatrix}$ and $\Sigma^I = \begin{pmatrix} \frac{1}{\omega - \frac{1}{\omega + i\frac{\Gamma}{2}}} & -\frac{1}{\omega}\frac{1}{\omega + i\frac{\Gamma}{2} - \frac{1}{\omega}} \\ -\frac{1}{\omega + i\frac{\Gamma}{2} - \frac{1}{\omega}}\frac{1}{\omega} & \frac{1}{\omega + i\frac{\Gamma}{2} - \frac{1}{\omega}} \end{pmatrix}$. The self-energy due to the extra substituent is $\Sigma^S = \begin{pmatrix} 0 & 0 \\ 0 & \frac{t^2}{\omega - \epsilon} \end{pmatrix}$. At $\omega = \epsilon$, $G^a_{12}(\omega)$ becomes zero (due to the bare advanced Green's function term becoming zero due to divergence of Σ^S_{22}), leading to the zero of the transmission function (termed as resonance zero). Another zero (multipath zero) of the transmission function can be identified at $\omega = 0$, where $(\Sigma^D_{12})^* + (\Sigma^I_{12})^* = -\frac{\omega}{\omega(\omega - i\frac{\Gamma}{2}) - 1}$ becomes zero, which can be interpreted as a result of destructive interference between direct and indirect paths. Another set of zeros (which are multipath zeros of net transmission function $T_L(\omega)$ at $\omega = \frac{\epsilon \pm \sqrt{\epsilon^2 + 2t^2}}{2}$ discussed above) does not have a simple interpretation in this procedure.

For analyzing zeros of transmission function $T_{14}(\omega) = -2\Gamma\,\mathrm{Im}[G^r_{11}(\omega)G^a_{14}(\omega)]$, for the current between sites 1 and 4, we project out sites 2, 3, and 5, to get

$$G^r_{11}(\omega) = \frac{1}{\omega + i\frac{\Gamma}{2} - \Sigma^I_{11} - \frac{\left(\Sigma^D_{14} + \Sigma^I_{14}\right)\left(\Sigma^D_{41} + \Sigma^I_{41}\right)}{\omega - \Sigma^I_{44}}} \tag{D7}$$

and

$$G^a_{14}(\omega) = \frac{1}{\omega - i\frac{\Gamma}{2} - \left(\Sigma^I_{11}\right)^* - \frac{\left[\left(\Sigma^D_{14}\right)^* + \left(\Sigma^I_{14}\right)^*\right]\left[\left(\Sigma^D_{41}\right)^* + \left(\Sigma^I_{41}\right)^*\right]}{\omega - \left(\Sigma^I_{44}\right)^*}} \times \left[\left(\Sigma^D_{14}\right)^* + \left(\Sigma^I_{14}\right)^*\right] \times \frac{1}{\omega - \left(\Sigma^I_{44}\right)^*}. \tag{D8}$$

$\Sigma^{D(I)}_{ab}$ are matrix elements of self-energies due to direct path $1 \to 4$ (indirect path $1 \to 2 \to 3 \to 4$) given by $\Sigma^D = \begin{pmatrix} 0 & -1 \\ -1 & 0 \end{pmatrix}$ and $\Sigma^I = \frac{1}{[(\omega + i\frac{\Gamma}{2})\{\omega(\omega - \epsilon) - t^2\} - (\omega - \epsilon)]}\begin{pmatrix} (\omega - \epsilon)(\omega + i\frac{\Gamma}{2}) & -(\omega - \epsilon) \\ -(\omega - \epsilon) & \omega(\omega - \epsilon) - t^2 \end{pmatrix}$. At $\omega = \frac{\epsilon \pm \sqrt{\epsilon^2 + 4t^2}}{2}$, $(\Sigma^D_{14})^* + (\Sigma^I_{14})^* = \frac{(\omega + i\frac{\Gamma}{2})\{\omega(\omega - \epsilon) - t^2\}}{[(\omega + i\frac{\Gamma}{2})\{\omega(\omega - \epsilon) - t^2\} - (\omega - \epsilon)]}$ becomes zero; hence $\omega = \frac{\epsilon \pm \sqrt{\epsilon^2 + 4t^2}}{2}$ are zeros of $T_{14}(\omega)$ (these zeros are a result of destructive interference between direct and indirect paths and hence can be termed as multipath zeros). Similarly to the $T_{12}(\omega)$ case, another set of zeros (at $\omega = \frac{\epsilon \pm \sqrt{\epsilon^2 + 2t^2}}{2}$) does not have a simple interpretation in this procedure.

[1] Y. Imry, *Introduction to Mesoscopic Physics* (Oxford University Press, Oxford, 2002).

[2] L. Pauling, The diamagnetic anisotropy of aromatic molecules, J. Chem. Phys. **4**, 673 (1936).

[3] N. Byers and C. N. Yang, Theoretical Considerations Concerning Quantized Magnetic Flux in Superconducting Cylinders, Phys. Rev. Lett. **7**, 46 (1961).

[4] M. Büttiker, Y. Imry, and R. Landauer, Josephson behavior in small normal one-dimensional rings, Phys. Lett. A **96**, 365 (1983).

[5] G. C. Solomon, C. Herrmann, T. Hansen, V. Mujica, and M. A. Ratner, Exploring local currents in molecular junctions, Nat. Chem. **2**, 223 (2010).

[6] A. Troisi, J. M. Beebe, L. B. Picraux, R. D. Van Zee, D. R. Stewart, M. A. Ratner, and J. G. Kushmerick, Tracing electronic pathways in molecules by using inelastic tunneling spectroscopy, Proc. Natl. Acad. Sci. USA **104**, 14255 (2007).

[7] D. Rai, O. Hod, and A. Nitzan, Magnetic field control of the current through molecular ring junctions, J. Phys. Chem. Lett. **2**, 2118 (2011).

[8] O. Hod, E. Rabani, and R. Baer, Magnetoresistance of nanoscale molecular devices, Acc. Chem. Res. **39**, 109 (2006).

[9] O. Hod, R. Baer, and E. Rabani, Magnetoresistance of nanoscale molecular devices based on Aharonov-Bohm interferometry, J. Phys.: Condens. Matter **20**, 383201 (2008).

[10] D. Rai, O. Hod, and A. Nitzan, Circular currents in molecular wires, J. Phys. Chem. C **114**, 20583 (2010).

[11] D. Rai, O. Hod, and A. Nitzan, Magnetic fields effects on the electronic conduction properties of molecular ring structures, Phys. Rev. B **85**, 155440 (2012).

[12] A. M. Jayannavar, P. Singha Deo, and T. P. Pareek, Current magnification and circulating currents in mesoscopic rings, Physica B **212**, 261 (1995).

[13] M. A. Davidovich, V. M. Apel, E. V. Anda, and G. Chiappe, Currents along ring arms with quantum dots: Kondo and Aharonov-Bohm effects, J. Magn. Magn. Mater. **320**, e246 (2008).

[14] R. Peierls, On the theory of diamagnetism of conduction electrons, Z. Phys. **80**, 763 (1933).

[15] H. Haug, A.-P. Jauho, and M. Cardona, *Quantum Kinetics in Transport and Optics of Semiconductors* (Springer, Berlin, 2008).

[16] J. Rammer, *Quantum Field Theory of Non-Equilibrium States* (Cambridge University Press, New York, 2007).

[17] Z. Y. Zeng, F. Claro, and A. Pérez, Fano resonances and Aharonov-Bohm effects in transport through a square quantum dot molecule, Phys. Rev. B **65**, 085308 (2002).

[18] A. Purkayastha, A. Dhar, and M. Kulkarni, Out-of-equilibrium open quantum systems: A comparison of approximate quantum master equation approaches with exact results, Phys. Rev. A **93**, 062114 (2016).

[19] S. R. de Groot and P. Mazur, *Non-Equilibrium Thermodynamics* (Dover, New York, 1984).

[20] C. Benjamin and A. M. Jayannavar, Equilibrium currents a quantum double ring system: A non-trivial role of system-reservoir coupling, Int. J. Mod. Phys. B **18**, 3343 (2004).

[21] M. Büttiker, Role of quantum coherence in series resistors, Phys. Rev. B **33**, 3020 (1986).

[22] M. Büttiker, Small normal-metal loop coupled to an electron reservoir, Phys. Rev. B **32**, 1846 (1985).

[23] L. Melville Milne-Thomson, M. Abramowitz, and I. A. Stegun, *Handbook of Mathematical Functions* (Dover, New York, 1972).

[24] Z.-M. Bai, M.-F. Yang, and Y.-C. Chen, Effect of inhomogeneous magnetic flux on double-dot Aharonov-Bohm interferometer, J. Phys.: Condens. Matter **16**, 2053 (2004).

[25] D. Sztenkiel and R. Świrkowicz, Interference effects in a double quantum dot system with inter-dot Coulomb correlations, J. Phys.: Condens. Matter **19**, 176202 (2007).

[26] O. Entin-Wohlman, Y. Imry, and A. Aharony, Persistent Currents in Interacting Aharonov-Bohm Interferometers and their Enhancement by Acoustic Radiation, Phys. Rev. Lett. **91**, 046802 (2003).

[27] O. Entin-Wohlman, Y. Imry, and A. Aharony, Effects of external radiation on biased Aharonov-Bohm rings, Phys. Rev. B **70**, 075301 (2004).

[28] T. P. Pareek, P. Singha Deo, and A. M. Jayannavar, Effect of impurities on the current magnification in mesoscopic open rings, Phys. Rev. B **52**, 14657 (1995).

[29] A. M. Jayannavar and P. Singha Deo, Persistent currents in the presence of a transport current, Phys. Rev. B **51**, 10175 (1995).

[30] T. Hansen, G. C. Solomon, D. Q. Andrews, and M. A. Ratner, Interfering pathways in benzene: An analytical treatment, J. Chem. Phys. **131**, 194704 (2009).

[31] L. Kouwenhoven, Coupled quantum dots as artificial molecules, Science **268**, 1440 (1995).

[32] T. Hatano, T. Kubo, Y. Tokura, S. Amaha, S. Teraoka, and S. Tarucha, Aharonov-Bohm Oscillations Changed by Indirect Interdot Tunneling via Electrodes in Parallel-Coupled Vertical Double Quantum Dots, Phys. Rev. Lett. **106**, 076801 (2011).